frontiers | Frontiers in Acoustics

TYPE Original Research
PUBLISHED 06 January 2025
DOI 10.3389/facou.2024.1498722

OPEN ACCESS

EDITED BY
Minghui Lu,
Nanjing University, China

REVIEWED BY
Frank Simon,
Office National d'Études et de Recherches Aérospatiale, France
Edith Roland Fotsing,
Polytechnique Montréal, Canada

*CORRESPONDENCE
Tenon Charly Kone,
TenonCharly.Kone@nrc-cnrc.gc.ca
Sebastian Ghinet,
sebastian.ghinet@nrc-cnrc.gc.ca

RECEIVED 19 September 2024
ACCEPTED 02 December 2024
PUBLISHED 06 January 2025

CITATION
Kone TC, Ghinet S, Panneton R and Grewal A (2025) Multi-objective optimization of structured material parameters for reducing broadband aircraft noise across various frequencies.
Front. Acoust. 2:1498722.
doi: 10.3389/facou.2024.1498722

Multi-objective optimization of structured material parameters for reducing broadband aircraft noise across various frequencies

Tenon Charly Kone[1]*, Sebastian Ghinet[1]*, Raymond Panneton[2] and Anant Grewal[1]

[1]Flight Research Laboratory Aerospace, National Research Council Canada, Ottawa, ON, Canada, [2]CRASH, Centre de Recherche Acoustique-Signal-Humain, Université de Sherbrooke, Boul de l'Université, Sherbrooke, QC, Canada

Introduction: Controlling broadband noise across the entire frequency spectrum, from low to high frequencies, remains a critical challenge in aerospace, transportation, and construction industries. Current acoustic metamaterials are effective primarily for low-frequency noise but suffer from narrow-band resonances that limit their application for broader-band noise attenuation.

Methods: This study introduces an innovative structured material system comprising a parallel assembly of structured materials and Helmholtz Resonators embedded within a fiberglass layer. A multi-objective optimization approach based on a surrogate model was employed to fine-tune the parameters of each structured material. The optimization process allowed precise grouping of individual resonant frequencies, thereby broadening the effective resonance frequency band to address low- and high-frequency noise.

Results: The proposed structured material system demonstrated significant broadband noise attenuation across a wide frequency range. The optimized configuration achieved effective noise reduction while adhering to practical implementation constraints, providing a feasible solution for industrial applications.

Discussion: This study underscores the importance of optimization in advancing noise control technologies. By overcoming the limitations of narrow-band resonances, the proposed approach achieves effective broadband noise attenuation, addressing critical challenges in aerospace, transportation, and construction. The integration of structured materials and Helmholtz Resonators, optimized using a surrogate model, broadens the resonance frequency band while meeting practical implementation requirements. These results highlight a viable and impactful solution for noise control across diverse industries.

KEYWORDS

metamaterial, optimization, broadband-noise, aircraft-noise, cabin noise, low-frequency

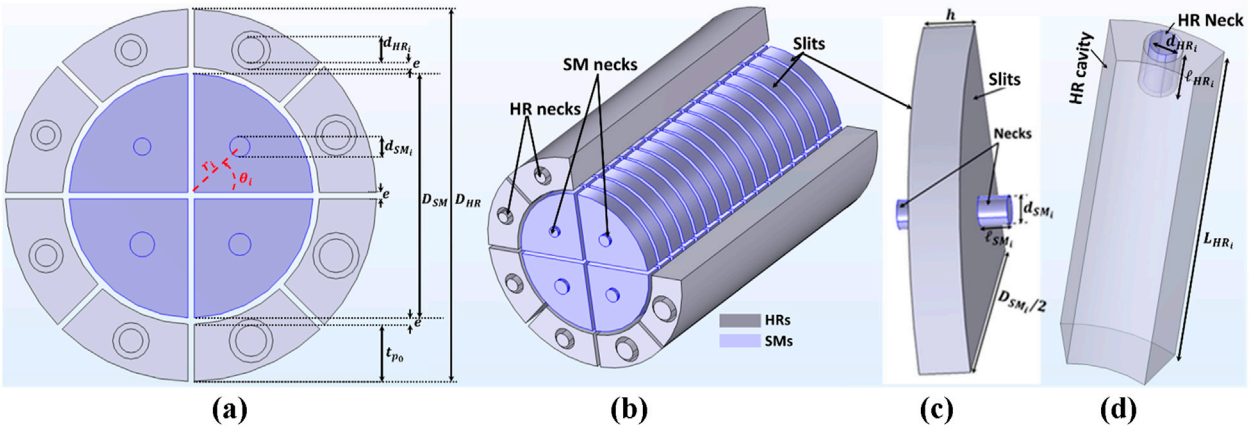

FIGURE 1
Metamaterial configuration under study: **(A)** Cross section, **(B)** Materials assembled without porous medium, **(C)** PUC of Structured Material, and **(D)** Inner HR.

1 Introduction

Attenuating a broad spectrum of noise sources, particularly at low frequencies within confined spaces, presents a significant challenge across various industries such as transportation, aeronautics, and building construction. The large wavelength characteristics of low-frequency noise impose fundamental design constraints, especially evident in the field of Unmanned Aerial Systems (UAS) noise mitigation. The primary noise source for UAS is propeller noise (Zhou and Fattah, 2017), which can be categorized into broadband noise and tonal noise (Kemp, 1932; Kurtz and Marte, 1970). Broadband noise arises from turbulence created by the interaction between the fluid and the propeller blade, while tonal noise results from rotor motion, with prominence at the harmonics of the propeller blade passing frequency.

While numerous techniques for controlling tonal noise exist, few simultaneously address both broadband and tonal noise effectively. For instance, the use of linear ducted propellers stands out as a method that enhances aerodynamic performance while protecting the blades from damage. Malgoezar et al. (2019) investigated propeller noise characteristics with a rigid duct through experimentation, revealing an increase in broadband noise, a decrease in the first harmonics, and an overall reduction in noise level upon duct introduction. Similarly Lu et al. (2016), explored the acoustic performance of both rigid and micro-perforated ducts, though the acoustic benefits were less significant than anticipated. Guo et al. (2021) developed a lined duct employing Helmholtz resonators with extended necks, achieving approximately 3 dB noise reduction within the 700–1,000 Hz range. In general, a well-designed ducted propeller can significantly enhance both aerodynamic and acoustic performances, particularly at high frequencies for broadband noise. However, the limited space available in propeller blade ducts restricts the integration of conventional materials such as Helmholtz Resonators (HRs). This type of liner is effective across a narrow frequency band, making it unsuitable for broadband noise reduction. Fortunately, new advancements in acoustic metamaterials offer greater potential for noise control.

Unlike traditional liners, which are limited to narrow frequency bands, the LEONAR (Simon, 2018; Simon, 2019; Jones et al., 2022) (Long Elastic Open Neck Acoustic Resonator) concept introduces an advanced design that can potentially extend the range of effective noise attenuation. This resonator consists of a perforated plate with holes connected to hollow, flexible, or rigid tubes that are inserted into a cavity and open at the end. The flexible tubes offer greater adaptability and allow for tuning of resonant frequencies, making the approach promising for applications requiring broadband noise control. Recent work by Simon (2024), Lafont et al. (2024) demonstrated the integration of the LEONAR concept in the acoustic coating applied to a hovering drone rotor, proposing optimized designs that achieved a wavelength-to-thickness ratio between 16 and 26, compared to the 4–8 range typical of classical resonators.

Kone et al. (2021a), Kone et al. (2022), Kone et al. (2021b), Kone et al. (2021c) proposed an alternative concept of structured materials, consisting of an assembly of four sub-metamaterials, each designed to group its lowest resonant frequencies together, forming a continuous frequency band for noise attenuation. This assembly effectively broadens the first resonant frequency band, attenuating up to 70% of noise levels. While other resonant frequency bands were also widened, the structured metamaterial achieved a noise attenuation of only 40% at these frequencies. Recent investigations (Kone et al., 2021c; Kone et al., 2020a) have shown that embedding these metamaterials within a layer of porous material, such as glass fiber, can further expand the absorption frequency ranges while maintaining good acoustic performance. Kone et al.'s studies revealed that the wavelength-to-thickness ratio for this type of metamaterial could exceed 30, providing an acoustic attenuation of 40% for frequencies above 200 Hz. Additionally, a second resonance frequency was observed with the structured materials, indicating potential for enhanced noise control.

Building on the work of Kone et al. (2024c), Kone et al. (2023), Kone et al. (2024d), this paper aims to propose a metamaterial

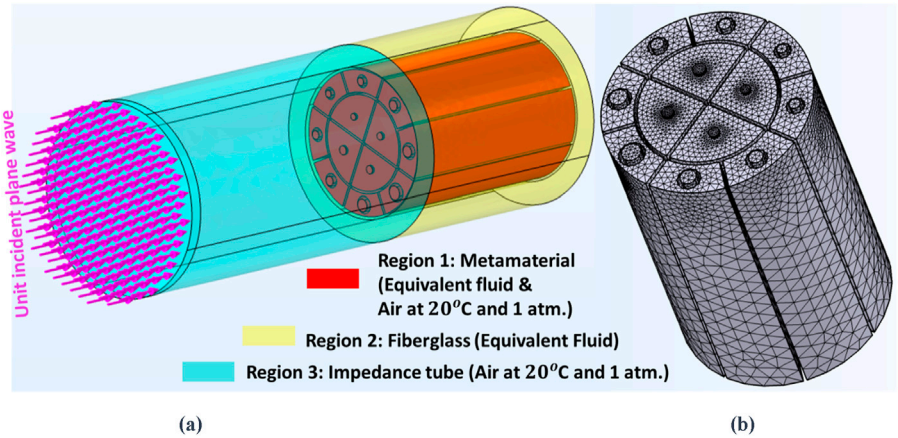

FIGURE 2
FEM model and mesh of the metamaterial connected to simulated impedance tubes for the hard-backed (SAC): **(A)** Model, and **(B)** mesh of Metamaterial without fiberglass layer.

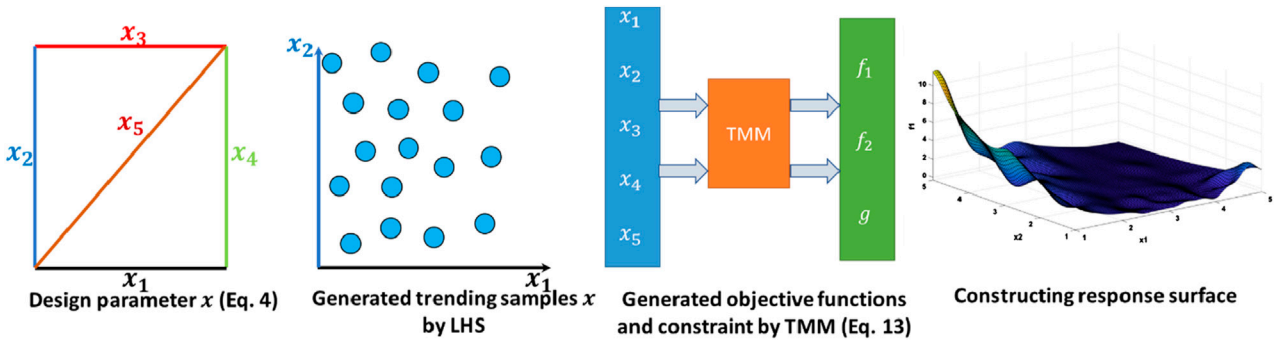

FIGURE 3
Surrogate modeling schema illustration.

resulting from a careful assembly of structured materials (SMs) and Helmholtz resonators (HRs) capable of simultaneously attenuating tonal and broadband noise at low frequencies. The developed metamaterial solution should be incorporated into the thermo-acoustic insulation of existing aircraft for an improved reduction of cabin noise. Moreover, the proposed solution had to be optimized not only for acoustic performance but also for low weight, and low fabrication costs. The challenge was therefore to select a concept that, through multi-variable optimization, would produce a noise reduction improvement and would rapidly reach a technology readiness level for integration on-board aircraft. The optimization approach used is based on the construction of the surrogate model (metamodel) from the design parameters. A surrogate model is a simplified model that approximates the behavior of a more complex system, allowing for faster evaluations and analysis. This model is built by adjusting the input (design parameters) – output (sound absorption coefficient and first resonance frequency) relationships to obtain a fast, high-fidelity response surface approximation. Constructing an accurate surrogate model requires adequate input–output samples (training samples) that can properly capture the characteristics of the response surface. Conventionally, training samples are generated by space-filling designs including Latin hypercube sampling (LHS) (Swiler and Wyss, 2004). The transfer matrix method (TMM) (Kone et al., 2020b; Verdiere et al., 2013) is employed to characterize the sound absorption coefficient of the metamaterials. Once the response surface model is established, the multiobjective genetic algorithm approach (MOGA) (Deb, 2001) available in the open source software Dakota (2020) is used to idenfy for the optimum design parameters of the metamaterial.

The results obtained are compared with those obtained from numerical simulations using the finite element method, providing a comprehensive analysis of their effectiveness in noise attenuation.

2 Materials

The metamaterials investigated in this paper were meticulously designed as an intricate assembly, incorporating four structured materials (SMs) and eight Helmholtz Resonators (HRs). These elements were precisely arranged in parallel and embedded within a layer of fiberglass (FGL), providing the resulting

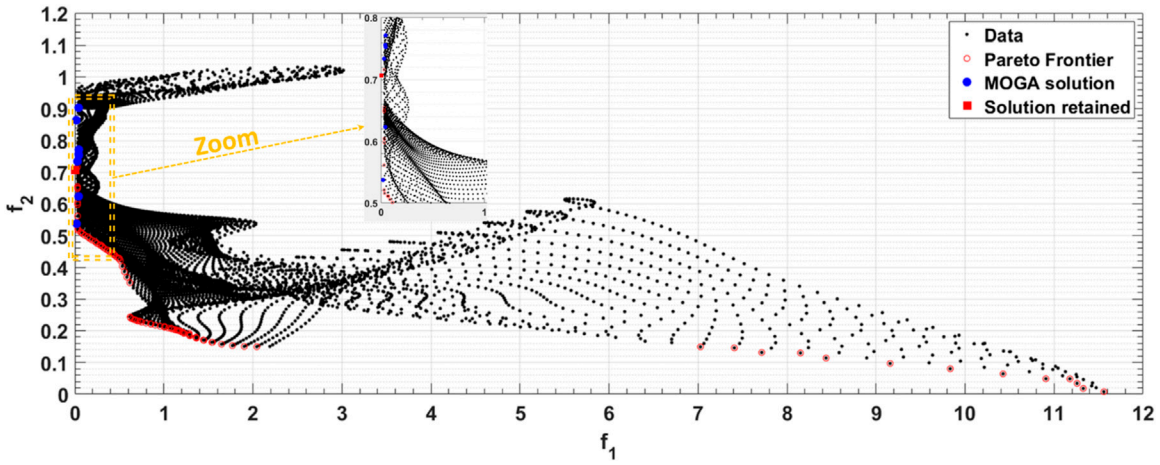

FIGURE 4
Samples of the objective functions, with the sound absorption coefficient (f_2) on the vertical axis and the dimensionless frequency (f_1) on the horizontal axis. The red circles indicate the points on the Pareto Front, the blue dots represent the MOGA solutions, and the red square dot marks the selected solution.

TABLE 1 Johnson-Champoux-Allard (JCA) parameters of the slit and neck and fiberglass, where η is the dynamic viscosity of air.

Materials	Viscous - characteristic lengths Λ	Thermal characteristic lengths Λ'	Tortuosity (α_∞)	Static airflow resistivity $\sigma\,(P_a.s/m^2)$	Open porosity Φ (%)
Slit	$h\ (mm)$	$h\ (mm)$	1	$12\eta/h^2\Phi$	100
Neck	$d_i/2\,(mm)$	$d_i/2\ (mm)$	1	$32\eta/d^2\Phi$	100
Fiberglass	85 (μm)	170 (μm)	1	20,709	85

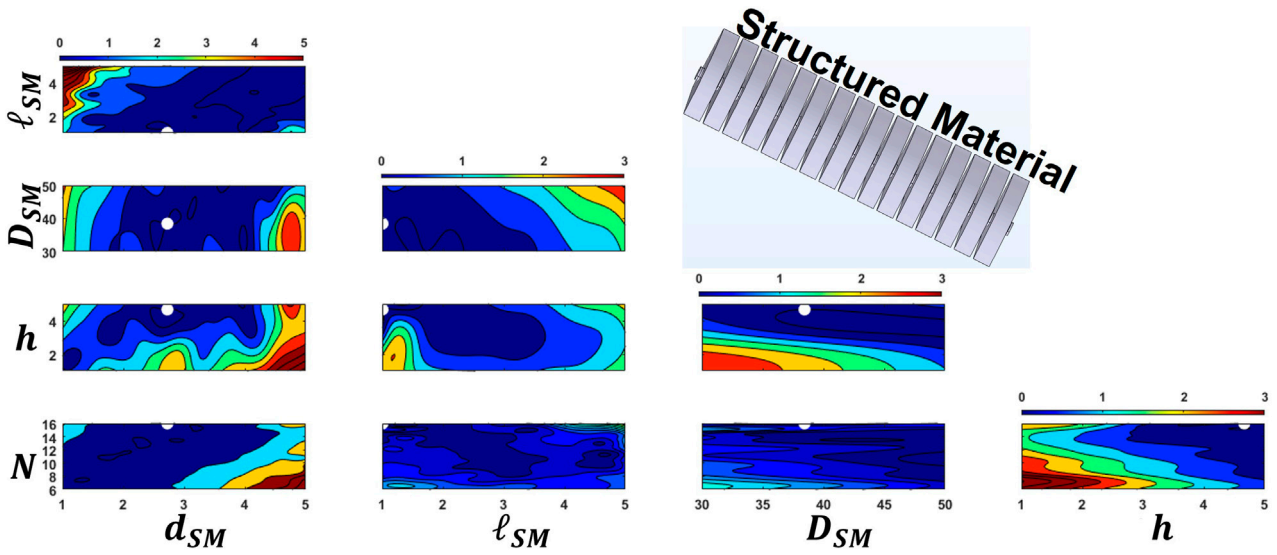

FIGURE 5
Non-dimensional resonnance frequency ($\boldsymbol{f_1}$) contour plots for the response surface of the surrogate model.

TABLE 2 Surrogate input variables and retain solution values in mm.

Input variables		Lower bound	Upper bound	Solution
x_1	Neck diameter	1	5	2.72
x_2	Neck thickness	1	5	1
x_3	Slit diameter	30	50	38.45
x_4	Slit thickness	1	5	4.67
x_5	Number of PUC	6	16	16

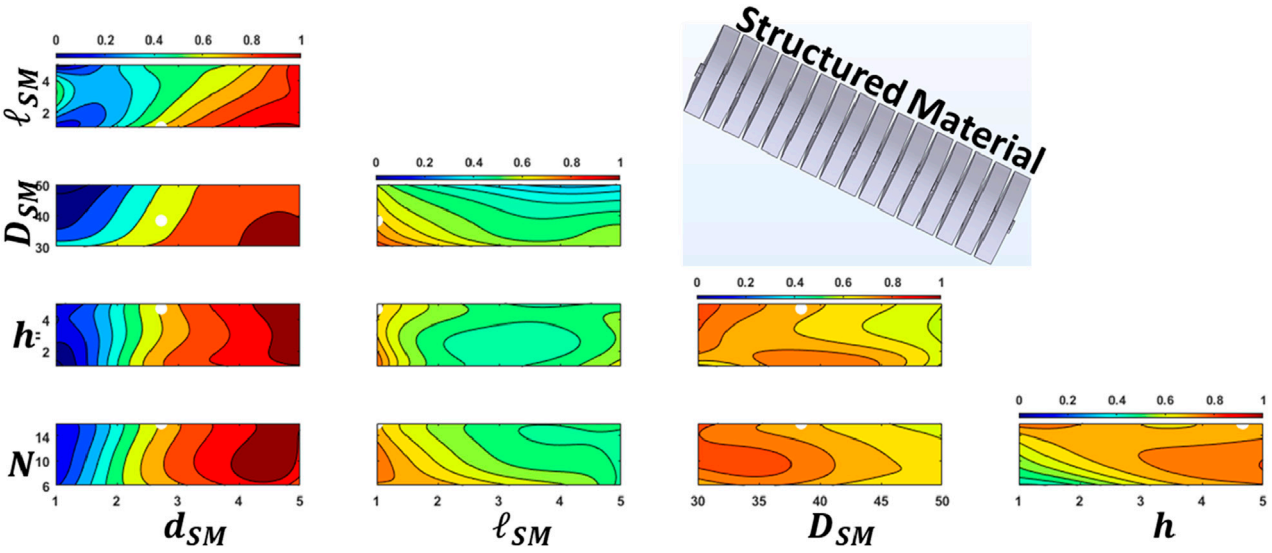

FIGURE 6
Sound Absorption Coefficient (f_2) contour plots for the response surface of the surrogate model.

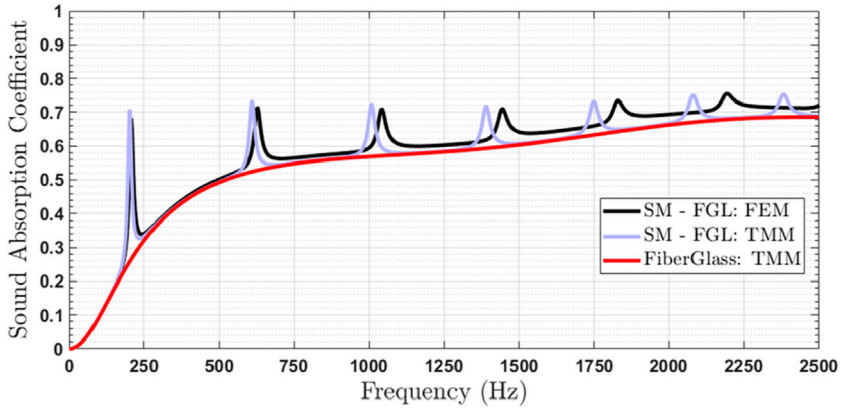

FIGURE 7
Sound absorption coefficient of one SM.

configuration with unique sound attenuation properties. The metamaterial, without the porous layer, had a cylindrical form with a diameter D_{HR} and a length L_{HR}. Each SM consisted of a series assembly of periodic unit cells (PUCs), where each PUC comprised a cylindrical neck with a diameter d_{SM_i} and height ℓ_{SM_i} (Figure 1A). This neck was followed by a cylindrical cavity quarter of

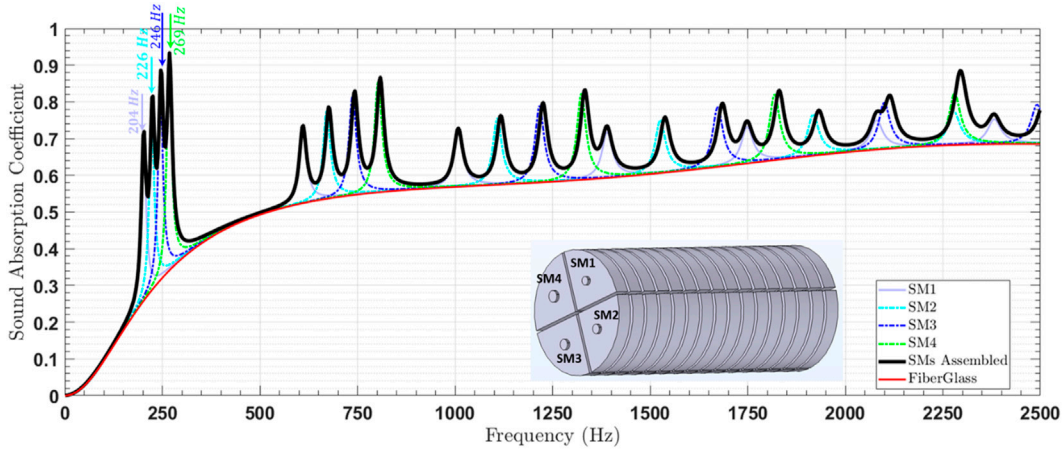

FIGURE 8
Sound absorption coefficient of four SMs assembled in parallel.

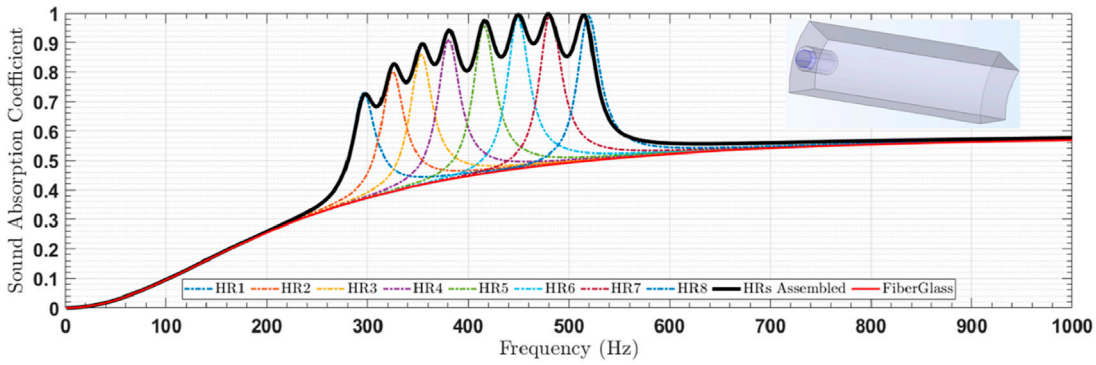

FIGURE 9
Sound absorption coefficient of eight HRs assembled in parallel.

TABLE 3 Eight HRs design parameter values in mm.

d_{HR_1}	d_{HR_2}	d_{HR_3}	d_{HR_4}	d_{HR_5}	d_{HR_6}	d_{HR_7}	d_{HR_8}
2.9	3.2	3.5	3.8	4.2	4.6	5.0	5.5

diameter D_{SM_i} and height h, referred to as a slit (small cavity), and ended with an identical neck (Figure 1C). The center of each neck linked to the i-th SM, was identified in the section plane of the metamaterial by the polar coordinates $(r_i = D_{SM_i}/4 + e, \theta_i = [1 + 2(i-1)]\pi/4)$ as illustrated in Figure 1A. The SM arrangements of the metamaterial are illustrated in Figure 1B. The assembly also incorporated a classic HR, denoted as an inner HR, depicted in Figure 1D. The inner HR featured a neck with a diameter d_{HR_i} and a length ℓ_{HR_i}. The cavities of the HRs were volume rings with interior diameters $D_{SM} + 2e$, exterior diameter $D_{SM} + 2e + 2t_{p0}$ and length L_{HR} enveloping the SMs. This ring was divided into eigth volumes. The necks of each HR were placed within the cavity and centered at the cavity section as shown in Figure 1D. To maximize the effectiveness of this metamaterial configuration, a multiobjective optimization approach was employed. Once the surrogate model was established, the MOGA available in the open-source software Dakota (Deb, 2001) was utilized to identify the optimal design parameters for the metamaterial. This optimization process ensured that the resulting configuration achieved significant noise attenuation across a broad frequency range, effectively addressing both low and high-frequency noise challenges, while leading in a very compact design.

This methodically designed and optimized metamaterial structure represents a novel and promising configuration for applications in aeronautics (propeller blade or aircraft cabin noise attenuation), ground transportation, and construction industries. The innovative integration of SMs and HRs, combined with the optimization process, provides a comprehensive and practical solution for broadband noise attenuation.

3 Modeling

Two complementary approaches were employed to characterize the acoustic properties of the materials described in Section 2. First,

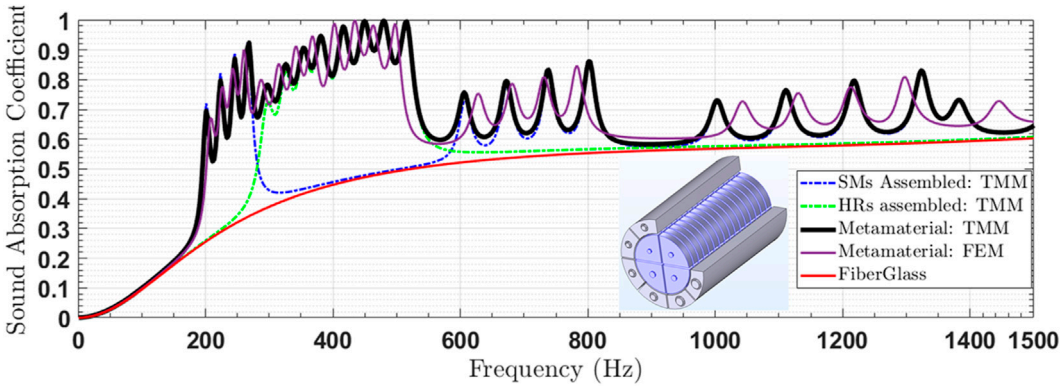

FIGURE 10
Sound absorption coefficient of the metamaterial.

the analytical approach based on transfer matrix methods (TMM) is presented in this section. This method is used to calculate the objective functions implemented in the optimization algorithms. Subsequently, the numerical approach is discussed, serving to validate and complement the findings using the analytical method.

3.1 Analytical approach

In order to quickly characterize the acoustic performance of the metamaterial, the transfer matrix method (TMM) has been adopted. The TMMs presented and developed in the work of Kone et al. (2024d); (Equation 7, 10, 11) are used in this study. These TMMs were used to build the global transfer matrix of the metamaterial under study. This global transfer matrix will allow the calculation of the sound absorption coefficient (backed by a rigid wall).

3.1.1 Metamaterial TMM

Knowing the transfer matrix of each element constituting the parallel assembly of the metamaterial (Equations 7, 10, 11 in Kone et al. (2024d)); the overall transfer matrix of the metamaterial is deduced from the parallel matrix method (PTMM) (Kone et al. (2021b), Swiler and Wyss, 2004) and is given by:

$$\mathbf{T_G} = -\frac{\mathbf{1}}{\sum \boldsymbol{r_i y_{i_{21}}}}\begin{bmatrix} \sum \boldsymbol{r_i y_{i_{22}}} & -\mathbf{1} \\ \sum \boldsymbol{r_i y_{i_{22}}} \sum \boldsymbol{r_i y_{i_{11}}} - \sum \boldsymbol{r_i y_{i_{12}}} \sum \boldsymbol{r_i y_{j_{21}}} & -\sum \boldsymbol{r_i y_{i_{11}}} \end{bmatrix} \tag{1}$$

where, $Y_i = \begin{bmatrix} y_{i_{11}} & y_{i_{12}} \\ y_{i_{21}} & y_{i_{22}} \end{bmatrix} = \frac{1}{T_{i_{12}}}\begin{bmatrix} T_{i_{22}} & -1 \\ 1 & -T_{i_{11}} \end{bmatrix}$, $i = \{SM_j, HR_k, FGL\}$, $j = 1,...,N_{SM}, k = 1,...,N_{HR}$, N_{SM} is number of SM present and N_{HR} is the number of HR present. $r_i = S_i/S_{total}$ is the surface ratio of element i over the total surface of the metamaterial.

3.1.2 Metamaterial acoustic properties

By defining the global matrix as $\mathbf{T_G} = [T_{G_{11}}, T_{G_{12}}; T_{G_{21}}, T_{G_{22}}]$, the normal-incidence sound absorption coefficient (SAC) of the hard-backed metamaterial and sound transmission loss (STL) are given by:

$$\mathbf{SAC} = \mathbf{1} - \left|\frac{\boldsymbol{T_{G_{11}} - T_{G_{21}} Z_o}}{\boldsymbol{T_{G_{11}} + T_{G_{21}} Z_o}}\right|^2 \tag{2}$$

3.2 Numerical approach

In this section only the model used to calculate the SAC is presented. Regarding the calculation of the STL, the reader will find a detailed description in Kone et al. (2024a). This subsection describes the analytical approach employed for SAC modeling. COMSOL Multiphysics was used for the prediction of the SAC of the metamaterial backed by a rigid wall at normal incidence. The frequency domain sound pressure modulus was used. The walls of each PUC were modelled as rigid. An impedance tube of diameter identical to the diameter of the metamaterial embedded in fiber glass, that is $D_p = D_{SM} + 4e + 2t_{p0} + 2t_p$, with an upstream air section of length $2D_P$ (Figures 2A, B), was used to predict the SAC of the metamaterial backed by a hard wall (hard-backed). The upstream side face of the metamaterial was placed at the origin. The model consisted of 3 regions numbered from 1 to 3. The first region (referred to as Region 1) comprised the metamaterial without the porous medium. The second region (referred to as Region 2) was composed only of the porous material. The last region (Region 3) was composed of the simulated impedance tube sections. In Region 1, the pressure acoustic (PA) module used the air properties at 20^oC and 1 Pa atmospheric pressure. The Johnson Champoux-Allard (JCA) (Champoux and Allard, 1991) model was used to represent the acoustics in the neck regions, the cavities (slit) and the fiberglass. The parameters required for COMSOL's JCA model for a circular neck, slit and fiberglass are given in Table 1. In Region 2, the PA module employed an equivalent fluid model based on the JCA approach. JCA material parameters of the fiberglass are given in Table 1. Finally, air at 20^oC and 1 atmospheric pressure was used in Region 3 with the PA module. Quadratic elements were used to discretize the entire model (Figure 4). In all regions, a fine mesh of the fluid dynamic type was employed. A unit incident plane wave was imposed upstream of the tube for both models. All solid walls were considered rigid and a no-slip boundary condition was used. In

this study the thickness of the glass fiber layer is fixed $t_p = t_{p_0} = 9$ mm and all the thicknesses of the solid walls are fixed at $e = 1$ mm

4 Optimization approach

In this section only the methodology to optimize a structured material (SM) constituting the metamaterials is presented. The problem is to find design parameters that allow good sound absorption at the first desired resonance frequency of the SM under the constraint that the total thickness of the SM is less than the maximum length L_{max}. This problem thus posed admits 2 objective functions and a geometric constraint. The first objective function f_1, is the frequency deviation of the first desired resonance frequency (f_0) of the SM. The objective of the problem is to minimize this function (f_1). This objective function is given by:

$$f_1 = \frac{|f - f_0|}{f_0} \tag{3}$$

where f is the computed frequency. As for the second objective function f_2, it is defined by the amplitude of the absorption coefficient (Equation 13) at the given resonance frequency f_0.

Five design parameters are necessary to design the SM described in section 2. These are the neck diameter d_{SM}, the neck thickness ℓ_{SM}, the diameter D_{SM} to describe the slit and the thickness of the slit h. The last design parameter is the number of PUCs, N needed to build the MS. Thus, the vector of design parameters $\boldsymbol{x}$, also called the optimization variables, is given by:

$$\boldsymbol{x} = [\boldsymbol{d_{SM}}, \boldsymbol{\ell_{SM}}, \boldsymbol{D_{SM}}, \boldsymbol{h}, \boldsymbol{N}] \tag{4}$$

Each of the components of the design vector is limited according to the geometric constraints of the available space. These inequalities are linear constraints of the optimization variables. The constraint governing the maximum thickness, is the nonlinear function g(x) and is defined as:

$$\boldsymbol{g(x)} = \frac{\boldsymbol{N(\ell_{SM} + h) + \ell_{SM}}}{\boldsymbol{L_{max}}} \leq \boldsymbol{1} \tag{5}$$

The optimization problem to solve is to find the variable vector x which minimizes f_1 and maximizes f_2 under linear and non-linear constraints. The optimization problem is defined by:

$$\begin{cases} \boldsymbol{min\ f_1(x)} \\ \boldsymbol{max\ f_2(x)} \\ \boldsymbol{x_{i_{min}} \leq x_i \leq x_{i_{max}}} \\ \boldsymbol{g(x) \leq 1} \end{cases} \tag{6}$$

were $x_i = d_{SM}, \ell_{SM}, D_{SM}, h, or\ N$.

Having defined the optimization problem, the next step involves constructing the response surface using surrogate modeling.

4.1 Surrogate model

The procedure of surrogate modeling is illustrated in Figure 3. This process begins with defining the input variables and target outputs. Input variables typically include the design parameters that influence the performance of the structured material (SM), such as neck diameter (d_{SM}), the neck thickness (ℓ_{SM}), the diameter (D_{SM}), slit thickness (h), and the number of PUC (N). The target outputs are the desired performance metrics, such as the sound absorption coefficient and the first resonance frequency. Next, training samples of these input variables are generated using design of experiments techniques. One common approach is the space-filling design, which ensures that the training samples cover the entire range of possible input values uniformly. This step is crucial as it ensures that the surrogate model will be accurate across the entire design space. Once the training samples are generated, computational model analysis is performed to obtain the corresponding target outputs. This involves the use of high-fidelity simulations to estimate how the SM performs under different configurations defined by the training samples. With the input-output data collected, a mathematical model is used to construct the surrogate model by fitting the relationships between the input variables and the target outputs. The surrogate model, also known as a response surface, approximates the behavior of the more complex computational model but at a significantly reduced computational cost. Surrogate models can be categorized into two main types: regression-based models and interpolation-based models. Regression-based models, such as polynomial functions, approximate the overall trend of the data and are typically used when a smooth approximation of the data is sufficient. Interpolation-based models, such as radial basis functions and kriging, provide an exact fit to the training data and are used when precise predictions at the training points are required (Dakota, 2020). This study utilizes the latter approach, which is implemented and detailed in the open-source software Dakota.

4.1.1 Kriging model

A Kriging model (Dakota, 2020), also known as Gaussian Process Regression, is a surrogate modeling technique used to predict the behavior of complex systems based on a limited number of observations. It creates a smooth approximation of a function by assuming that the unknown function follows a Gaussian process, characterized by a mean and a covariance function. A Kriging emulator, $\hat{f}(\boldsymbol{x})$, consist of a trend function $\mu(\boldsymbol{x})$ plus a Gaussian error model $\sigma^2 \psi(x_i, x_j)$

$$\hat{\boldsymbol{f}}(\boldsymbol{x}) = \boldsymbol{\mu}(\boldsymbol{x}) + \boldsymbol{\sigma^2}\, \boldsymbol{\psi}(\boldsymbol{x_i}, \boldsymbol{x_j}) \tag{7}$$

4.1.2 Trend function

In a Kriging process, the trend function ($\mu(\boldsymbol{x})$) models the underlying deterministic trend of the data. It represents the expected value of the response variable given the input variables. The trend function can take various forms, ranging from a simple constant to a complex polynomial. Incorporating a trend function allows the Kriging model to account for systematic variations in the data, improving the accuracy of predictions. In this study, the quadratic trend function is used and is given by:

$$\boldsymbol{\mu(x)} = \boldsymbol{\beta_0} + \sum_{i=1}^{p} \boldsymbol{\beta_i x_i} + \sum_{i=1}^{p} \sum_{j=1}^{p} \boldsymbol{\beta_{ij} x_i x_j} \tag{8}$$

The constructed surrogate model is then used in the optimization process. By evaluating the surrogate model, the optimization algorithm can efficiently explore the design space to find the optimal set of parameters that minimizes the first objective

function f_1 and maximizes the second objective function f_2. This process significantly reduces the computational cost compared to directly using the high-fidelity models in the optimization loop.

4.2 Multiobjective genetic optimization algorithm using a surrogate model

In this subsection, the methodology for optimizing the structured material (SM) using a multiobjective genetic algorithm (MOGA) in conjunction with surrogate models described in subsection 4.1. The MOGA is an optimization technique inspired by the principles of natural evolution and genetic processes. Unlike traditional genetic algorithms that focuses on a single objective function, MOGA optimizes multiple conflicting objective functions simultaneously. This approach is particularly useful in engineering and design problems where trade-offs between different performance metrics are required. MOGA uses a population of candidate solutions to explore the search space. This allows the algorithm to maintain diversity and identify multiple Pareto optimal solutions in a single run. Solutions are selected based on their fitness, which is determined by their performance on multiple objectives. Techniques such as Pareto ranking and crowding distance are used to maintain a diverse set of high-quality solutions.

5 Results

In this section, the optimization results are analyzed and interpreted. First, the sound absorption coefficient (SAC) of the optimized structured material (SM) configuration is presented. Next, the SAC of the four assembled SMs and the eight assembled Helmholtz Resonators (HRs) is analyzed. Finally, the SAC of the complete metamaterial is evaluated.

5.1 Interpretation of optimization results

This section aims to solve the optimization problem defined in Equation 7, which seeks to identify the design parameters of a structured material (SM) that achieves high absorption performance at a first resonance frequency close to $\boldsymbol{f_o = 200}$ Hz. Additionally, the thickness of the SM must not exceed $\boldsymbol{L_{Max} = 100}$ mm. To construct the metamodel, Dakota's Gaussian process model with a quadratic trend function was utilized, as depicted in Figure 3. The input variables and their respective ranges are detailed in Table 2. The outputs of this model were calculated using the analytical approach described in . After obtaining the response surface, Dakota's MOGA approach was employed to identify candidate solutions that meet the objective criteria. The optimal solution selected from the optimization process is presented in the final column of Table 2. The sound absorption coefficient measures a material's ability to absorb sound at various frequencies, providing insights into noise mitigation performance. By analyzing this coefficient across a range of frequencies, we can evaluate how well the material performs. The Pareto front illustrates the trade-offs between maximizing sound absorption and meeting other design criteria. Each point on the front represents a balanced solution, with the optimal choice offering the best absorption across the desired frequency range while fulfilling additional key objectives. These results are confirmed by the Pareto front in Figure 4, which displays both the solutions generated by the MOGA approach and the optimal solution retained in this study.

The validation of the surrogate model was carried out using 100 samples, all derived from solutions predicted by the MOGA approach. This number of samples was selected to ensure a comprehensive evaluation of the surrogate model's predictive capabilities across a diverse range of scenarios. The accuracy of the surrogate model is substantiated by an error threshold defined as $\frac{|f_{i_{MOGA}} - f_{i_{TMM}}|}{f_{i_{TMM}}} \leq 2\%\ i = 1\ or\ 2$, $f_{i_{MOGA}}$ represents the predictions of the objective functions obtained from the surrogate model and $f_{i_{TMM}}$ denotes the calculations of the objective functions using the TMM. This error threshold indicates that the predictions from the surrogate model deviate from the TMM results by no more than 2%, demonstrating a satisfactory level of accuracy for practical applications. The ability of the surrogate model to produce reliable predictions within this error margin is crucial for its use in optimizing the design and performance of the metamaterials. Overall, this validation process confirms the surrogate model's effectiveness and its potential to streamline computational efforts in future research endeavors by reducing reliance on more time-consuming methods like TMM.

The results indicate that the optimized design parameters successfully achieve the desired absorption performance at the specified resonance frequency while adhering to the thickness constraint. This demonstrates the effectiveness of the surrogate modeling and optimization approach in designing structured materials with targeted acoustic properties.

The design parameter values from the solution, along with the variable ranges, were used to generate contour plots for both objective functions constructed using the surrogate model. Figures 5, 6 each displays a contour plot, illustrating the first SM's resonance frequency and its absorption amplitude, respectively. In each subplot, two of the five design variables are varied, while the remaining variables are fixed at the values from the solution. These contour plots reveal the non-linear response surface of each objective function. The white dots on the subfigures represent the solutions of the optimization problem. The contour levels of the objective functions at these points are 0.005 for the first function (Figure 5) and 0.7 for the second objective function (Figure 6). These results demonstrate the reliability of the response surface model in addressing the optimization problem.

5.2 Sound absorption coefficient of optimized SM

The structured material (SM), derived from solving the optimization problem and detailed in the last column of Table 2, was evaluated for its sound absorption performance validation. Figure 7 illustrates the sound absorption coefficient at normal incidence for the SM with a rigid bottom, as determined both analytically (using) and numerically (as described in Section 2). The results from both methods are in close agreement. A slight frequency shift is observed from the third resonance frequency onward of the SM. The authors believe that this is due to the

approximation on the equivalent diameter of the SM slit made (Kone et al., 2024d). Since our objective is on the first resonance frequency, this influences very little our analysis. The first significant absorption frequency occurs around $f_o = 200$ Hz, which corresponds to an objective function value of $f_1 = 0.005$ and an absorption performance of 70% i.e., $f_2 = 0.7$.

5.3 Sound absorption coefficient of assembled SMs

The metamaterials consist of an assembly of four SMs in parallel, complemented by eight HRs. Each SM's design parameters are identical except for the diameter of the neck of each Periodic Unit Cell (PUC). The objective is to have the first resonance frequencies of all four SMs closely spaced yet distinct. For instance, let SM1 represent the optimized configuration with the design parameters specified in the last column of Table 2, featuring a neck diameter of $d_{SM_1} = 2.72$ mm. The neck diameters for the other SMs are calculated using $d_{SM_i} = d_{SM_1} + (i-1) \times 0.3$ mm, where $i = 2, 3, and\ 4$. The remaining four parameters are kept identical to those listed in the last column of Table 2. Figure 8 illustrates the sound absorption coefficient (SAC) for each individual SM as well as for the combined assembly. The resonance frequencies of the four SMs are closely spaced, resulting in an absorption performance of at least 55% over a frequency range of 88 Hz, starting from 197 Hz. However, in the frequency range from 286 Hz to 500 Hz, the absorption performance of the assembled SMs falls below 50 %. To address this issue and improve absorption in this frequency range, Helmholtz resonators (HRs) are incorporated into the design.

Glass fiber is typically effective in attenuating high frequencies. In this study, its impact is observed at frequencies below 250 Hz (see Figures 7, 8), where it achieves an absorption performance of over 32%. Without the glass fiber layer, absorption at the second first resonance frequency (around 611 Hz) reaches only 21%, whereas the addition of the glass fiber increases it to 73%, resulting in a 52% improvement due to the contribution of the glass fiber.

5.4 Sound absorption coefficient of assembled HRs

The Helmholtz resonators (HRs) incorporated into the design all have identical cavity volumes and the same neck length, defined by $\ell_{HR} = (N-14)(l+h)+l$. The only variable parameter among the HRs is the neck diameter, which was determined using Equation 3 and the resulting values are listed in Table 3. Figure 9 shows the SAC at normal incidence for each of the eight HRs. The HRs with the smallest neck diameter have the lowest resonance frequency, which is higher than the highest first resonance frequency of the SMs. Despite this, the resonance frequencies of the eight HRs are closely spaced. This configuration enables the SAC of the assembled system to achieve an absorption performance of at least 70 % over a frequency range of 142 Hz, starting from 291 Hz. The introduction of HRs effectively improves the absorption performance in the previously problematic frequency range of 283 Hz to 536 Hz, enhancing the overall sound absorption efficiency of the metamaterial system.

5.5 Sound absorption coefficient of metamaterial

The structured materials (SMs) and Helmholtz resonators (HRs) were assembled in parallel to create the metamaterial for this study. The normal incidence sound absorption coefficient (SAC) of the metamaterial was determined using the TMM approach, as described by . These results were compared with those obtained from finite element method (FEM) simulations performed using COMSOL Multiphysics, as shown in Figure 10.

The SAC values derived from the analytical TMM model were found to be in close agreement with the FEM simulation results, validating the accuracy of the TMM approach. However, a slight frequency shift is observed from the resonance frequencies of the SM. The authors believe that this is due to the approximation on the equivalent diameter of the SM slit made (Kone et al., 2024d). Further investigation is needed to understand this discrepancy. However, it has very little impact on our study. This innovative configuration led to significantly improved acoustic performance, achieving an absorption rate of 60% for frequencies above 197 Hz. Furthermore, the metamaterial exhibited four distinct resonance frequencies, corresponding to the second resonance frequencies of each structured material, with these frequencies occurring around 596 Hz.

In the detailed analysis of the metamaterial's acoustic properties, three distinct absorption frequency bands were identified, demonstrating the material's capability to attenuate sound effectively across a broad frequency range (Figure 10). The first absorption band, which spans from 196 to 289 Hz, achieved performance levels above 50%, indicating significant sound attenuation in the lower frequency range. The third band, extending from 596 to 845 Hz with absorption performance exceeding 60%, was also linked to strong attenuation characteristics. Both of these bands emerged from the parallel assembly of three distinct structured metamaterial configurations, which worked in tandem to broaden the resonance frequencies, enabling more effective suppression of low-frequency noise. This arrangement facilitated the exploitation of multiple resonant mechanisms that overlapped to produce a more comprehensive attenuation profile, as illustrated in Figures 8, 10.

The intermediate absorption band, covering the range from 293 to 536 Hz, exhibited even higher absorption performance, with levels surpassing 70%. This enhanced absorption was primarily attributed to the parallel configuration of eight Helmholtz resonators. The design leveraged the individual resonance characteristics of each resonator, creating a cumulative effect that widened the frequency range of significant noise reduction. The resonators' ability to target specific frequencies made them particularly suitable for addressing mid-range sound attenuation, as depicted in Figures 9, 10.

Moreover, the metamaterial demonstrated a wavelength-to-thickness ratio of approximately 18, placing it within the optimal range for acoustic metamaterial performance as proposed by Simon (2024), Lafont et al. (2024). This ratio indicates that the metamaterial achieves a compact form factor while maintaining high efficiency in sound absorption, aligning with the trend in modern acoustic engineering to develop thinner, lightweight materials that do not compromise on performance. The results

underscore the potential of combining structured metamaterials with classical resonator designs to create hybrid configurations that offer superior noise control across a wide frequency spectrum, thus meeting stringent industrial requirements for low-frequency noise management.

6 Conclusion

In conclusion, this study has introduced and characterized thin acoustic metamaterials designed to effectively attenuate both tonal and broadband noise at low frequencies The optimization of the structured materials (SMs) and Helmholtz Resonators (HRs) has demonstrated significant potential for noise control across various industrial applications, including aeronautics, transportation, and construction.

The optimization approach successfully fine-tuned the design parameters of the SMs to achieve an absorption performance of at least 55% across a frequency range from 197 Hz to 285 Hz. To address performance deficiencies in the frequency range of 286 Hz to 500 Hz, HRs were incorporated, leading to an improved absorption rate of at least 70 % from 293 Hz to 536 Hz. This integration enhanced the overall acoustic performance of the metamaterial.

Analytical validation using the transfer matrix method (TMM) and comparative analysis with COMSOL simulations confirmed the robustness and computational efficiency of our approach. The TMM not only accurately predicted key metrics such as the Sound Absorption Coefficient (SAC) but also enabled rapid design optimization, which is crucial for tailoring metamaterials to meet specific acoustic performance requirements. The study underscores the dual benefits of these metamaterials in attenuating noise and enhancing sound transmission loss, making them versatile solutions for mitigating environmental noise pollution and improving acoustic comfort. The practical implications are significant, offering various industries a pathway to deploy efficient and customized noise control solutions rapidly and effectively.

Despite the acoustic advantages of this metamaterial, several aspects still require further investigation. One important factor is the weight of the metamaterial, which needs to be carefully studied to ensure its practicality in real-world applications.

Future research should focus on balancing acoustic performance with material density and structural design to achieve an optimal solution that meets both acoustic and weight constraints. Continued exploration of additional configurations and materials could optimize performance across broader frequency ranges and address specific industrial noise challenges more comprehensively.

Data availability statement

The raw data supporting the conclusions of this article will be made available by the authors, without undue reservation.

Author contributions

TK: Conceptualization, Data curation, Formal Analysis, Funding acquisition, Investigation, Methodology, Project administration, Resources, Software, Supervision, Validation, Visualization, Writing–original draft, Writing–review and editing. SG: Investigation, Methodology, Resources, Supervision, Validation, Writing–review and editing. RP: Writing–review and editing. AG: Investigation, Methodology, Resources, Supervision, Validation, Writing–review and editing.

Funding

The author(s) declare that no financial support was received for the research, authorship, and/or publication of this article.

Conflict of interest

The authors declare that the research was conducted in the absence of any commercial or financial relationships that could be construed as a potential conflict of interest.

Publisher's note

References

Champoux, Y., and Allard, J. (1991). Dynamic tortuosity and bulk modulus in air-saturated porous media. *J. Appl. Phys.* 70 (4), 1975–1979. doi:10.1063/1.349482

Dakota, A. *Multilevel parallel object-oriented framework for design optimization, parameter estimation, uncertainty quantification, and sensitivity analysis: version 6.13 user's manual, sand2020-12495 unlimited release* (2020).

Deb, K. (2001). *Multi-objective optimization using evolutionary algorithms*. Hoboken, USA: John Wiley and Sons.

Guo, J., Zhou, T., Fang, Y., and Zhang, X. (2021). Experimental study on a compact lined circular duct for small-scale propeller noise reduction. *Appl. Acoust.* 179, 1–10. doi:10.1016/j.apacoust.2021.108062

Jones, M. G., Simon, F., and Roncen, R. (2022). Broadband and low-frequency acoustic liner investigations at NASA and ONERA. *AIAA J.* 60, 2481–2500. doi:10.2514/1.J060862

Kemp, C. F. B. (1932). Some properties of the sound emitted by airscrews. *Proc. Phys. Soc.* 44, 151–165. doi:10.1088/0959-5309/44/2/305

Kone, T. C., Ghinet, S., Dupont, T., Panneton, R., Grewal, A., and Wickramasinghe, V. (2020b). Characterization of the acoustic properties of complex shape metamaterials in *Proceedings of INTER-NOISE*, 23–26.

Kone, T. C., Ghinet, S., Panneton, R., Dupont, T., and Grewal, A. (2020b). Multi-tonal low frequency noise control using Helmholtz resonators with complex cavity designs for aircraft cabin noise improvement. *Inter. Noise. Proc. Inter-Noise*, 263(2), 3975–3986. doi:10.3397/in-2021-2569

Kone, T. C., Ghinet, S., Panneton, R., and Grewal, A. (2020a). Characterization of the acoustic properties of complex shape metamaterials in *Proceedings of INTER-NOISE*, 261.

Kone, T. C., Ghinet, S., Panneton, R., and Grewal, A. (2020c). Optimization of metamaterials with complex neck shapes for aircraft cabin noise improvement.

Inter. Noise. Proc. INTER-NOISE, 263(2), 3963–3974. doi:10.3397/in-2021-2567

Kone, T. C., Ghinet, S., Panneton, R., and Grewal, A. (2023). Method for characterizing the acoustic properties of thin metamaterials capable of attenuating broadband noise at low frequencies in Proceedings of AWC 2023 conference, 51.3.

Kone, T. C., Ghinet, S., Panneton, R., and Grewal, A. (2024a). Mitigating low-frequency broadband aircraft noise through an assembly of structured acoustic materials. *Proc. Mtgs. Acoust.* 54, 030001. doi:10.1121/2.0001897

Kone, T. C., Ghinet, S., Panneton, R., and Grewal, A. (2024b). Structured acoustic materials for mitigating low-frequencybroadband aircraft noise: transfer matrix method in *Proceedings of INTER-NOISE* (Nante, France), 25–29 August.

Kone, T. C., Ghinet, S., Panneton, R., and Grewal, A. (2024c). Broadband low frequency noise attenuation using thin acoustic metamaterials for aircraft cabin noise mitigation in *Inter-noise 2023 – 52nd international congress and exposition on noise control engineering, 2023, chiba, greater*. Tokyo, Japan.

Kone, T. C., Ghinet, S., Panneton, R., and Grewal, A. (2024d). Broadband aircraft noise attenuation across low and high frequencies using structured materials in *Proceedings of noise-con 2024* (New Orleand, LA: US).

Kone, T. C., Ghinet, S., Panneton, R., Grewal, A., Laly, Z., and Mechefske, C. (2022). Control and broadening of multiple noise frequencies using an assembly of sub-metamaterials connected by membranes for aircraft noise mitigation. *Inter. Noise. Proc. INTER-NOISE*, 265(3), 4607–4615. doi:10.3397/in_2022_0663

Kone, T. C., Lopez, M., Ghinet, S., Dupont, T., and Panneton, R. (2021a). Thermoviscous-acoustic metamaterials to damp acoustic modes in complex shape geometries at low frequencies. *JASA* 150 (3), 2272–2281. doi:10.1121/10.0006441

Kurtz, D. W., and Marte, J. E. (1970). *A review of aerodynamic noise from propellers, rotors, and lift fans*. California: California Institute of Technology.

Lafont, V., Sebbane, D., and Simon, F. (2024). "Feasibility of an acoustic liner applied to a fenestron: experimentation, inter-noise 2024," in 53rd International Congress and Exposition on Noise Control Engineering, Nantes, France.

Lu, Z., Debiasi, M., and Khoo, B. C. (2016). "Acoustic characteristics of a multi-rotor MAV and its noise reduction technology," in INTER-NOISE and NOISE-CON congress and conference proceedings, Hamburg, Germany.

Malgoezar, A. M., Vieira, A., Snellen, M., Simons, D. G., and Veldhuis, L. L. (2019). Experimental characterization of noise radiation from a ducted propeller of an unmanned aerial vehicle. *Int. J. Aeroacoustics* 18, 372–391. doi:10.1177/1475472x19852952

Simon, F. (2018). Long elastic open neck acoustic resonator for low frequency absorption. *J. Sound. Vib.* 421, 1–16. doi:10.1016/j.jsv.2018.01.044

Simon, F. (2024) Design and evaluation of an acoustic liner applied to a UAV ducted rotor in hover in *Inter-noise 2024 – 53rd international Congress and Exposition on noise control engineering, 2024*. Nantes France.

Simon, F. (2019). *Garniture surfacique pour absorption acoustique*.

Swiler, L. P., and Wyss, G. D. (2004). *A user's guide to Sandia's Latin hypercube sampling software: LHS UNIX library and standalone version*. Albuquerque, NM: Sandia National Laboratories. Technical Report SAND04-2439.

Verdiere, K., Panneton, R., Elkoun, S., Dupont, T., and Leclaire, P. (2013). Transfer matrix method applied to the parallel assembly of sound absorbing materials. *JASA* 134, 4648–4658. doi:10.1121/1.4824839

Zhou, T., and Fattah, R. (2017). Tonal noise acoustic interaction characteristics of multi-rotor vehicles in 23rd AIAA/CEAS aeroacoustics conference. AIAA 2017-4054.